



# Study of Spatio-Temporal Character of Frequency Combs Generated by Quantum Cascade Lasers

Nathan Henry , David Burghoff, Qing Hu , and Jacob B. Khurgin 

**Abstract**—Free-running quantum cascade lasers (QCLs) show a natural tendency to operate in the multimode regime as a result of both spatial and spectral hole burning. While multimode operation by itself is far from unusual, what distinguishes QCLs from other lasers is that the phases of the individual modes in them can be locked in the absence of any additional intracavity elements, thus forming frequency combs (FCs) that have many practical applications. Unlike typical FCs produced in mode-locked lasers or microcavities, the temporal shape of a QCL FC is not a short pulse but rather a combination of frequency and (to a lesser extent) amplitude modulated signals, the origin of which is not obvious. In this paper, we develop a theory aimed at explicating the most recent experimental measurements of temporal characteristics of QCL FCs. We identify spatial hole burning as the root cause of frequency modulation and show that, in addition to previously analyzed rapid, pseudo-random frequency modulation, the experimentally observed long linearly chirped signal can also alleviate spatial hole burning efficiently. We find that in the absence of spectral hole burning, a linearly chirped regime has the lowest threshold. Furthermore, we show that for relatively weak frequency modulation, amplitude modulation should also arise as confirmed experimentally. The result of this paper is a first step toward reliably engineering FCs with specified characteristics in mid IR and THz regions.

**Index Terms**—Quantum cascade lasers, frequency combs, hole burning.

## I. INTRODUCTION

**O**PTICAL frequency combs (FCs) generated by lasers, often in combination with non-linear, devices such as microresonators, have revolutionized the precision at which we are able to measure time, frequency, and distance [1]. Directly measuring radiation frequency offers a much higher resolution, as time can be measured with a higher accuracy than distance, and conversion between frequency and wavelength can be done

Manuscript received February 16, 2019; revised May 16, 2019 and July 9, 2019; accepted July 10, 2019. Date of publication July 17, 2019; date of current version August 2, 2019. This work was supported in part by DARPA SCOUT Program (W31P4Q161001). (Corresponding author: Nathan Henry.)

N. Henry and J. B. Khurgin are with the Whiting School of Engineering, Johns Hopkins University, Baltimore, MD 21218 USA (e-mail: nhenry7@jhu.edu; jakek@jhu.edu).

D. Burghoff was with the Massachusetts Institute of Technology, Cambridge, MA 02139 USA. He is now with the College of Engineering, University of Notre Dame, Notre Dame, IN 46556 USA (e-mail: dburghoff@nd.edu).

Q. Hu is with the Massachusetts Institute of Technology, Cambridge, MA 02139 USA (e-mail: qhu@mit.edu).

This paper has supplementary downloadable material available at <http://ieeexplore.ieee.org>, provided by the authors.

Color versions of one or more of the figures in this paper are available online at <http://ieeexplore.ieee.org>.

Digital Object Identifier 10.1109/JSTQE.2019.2929222

without much concern for accuracy degradation [2]. While FC generation in the visible and near-infrared (IR) has shown substantial progress over the last decade, FC generation is currently much less viable in the mid-IR and THz regimes, where their applications are mostly in precise spectroscopy of rotational and vibrational resonances [2].

Typically, FCs are generated either with mode-locked laser pulses or by sending coherent light through a non-linear resonator [3]–[6]. However, there is a lack of materials available to achieve this at longer wavelengths and current approaches typically include non-linear frequency conversion [7], at the expense of overall efficiency. It is hoped that this method can be improved upon by the FC generating Quantum Cascade Laser (QCL).

QCLs [8] are a ubiquitous source of coherent radiation in the mid-IR to THz regions of the spectrum. However, passive mode-locking is hard to achieve in QCLs because of their inherently short gain recovery time (upper laser level lifetime  $\tau_{21}$ ) which is typically on the order of 1 ps and is much shorter than the cavity round trip time  $\tau_{rt} \sim 100$  ps. Despite this difficulty, experimental evidence has shown that FCs are indeed generated by free-running QCLs [9], [10], i.e., without introduction of any additional active or passive elements into the cavity, a rather fortuitous turn of events. Given proper dispersion compensation and a broadband gain medium, QCLs operating throughout the mid-IR and THz regions reliably generate coherent FCs. However, in the temporal domain these FCs look quite different from the more familiar FCs produced by the mode-locked lasers and/or microresonators. While the temporal shape of the latter is a simple periodic train of short pulses, the QCL FC is continuous, (i.e., not pulsed) albeit with some amplitude modulation (AM), and always shows strong frequency modulation (FM).

As a first attempt to explicate this behavior, a theoretical model was developed via a perturbative solution of the Maxwell Bloch equation in the frequency domain (FD) [11], illustrating that frequency modulation is indeed a natural consequence of spatial hole burning (HB) in a broad gain medium (from which multimode operation follows) and a short gain recovery time which favors constant intensity. This combination of multimode operation with constant intensity is a signature of frequency modulation. The above theoretical model predicts a pseudo-random frequency modulation of the laser with an average period of oscillations commensurate with the gain recovery time and an amplitude comparable with the gain bandwidth. However, this FD model did not explain conclusively why pseudo-random FM is preferable to periodic FM, and it also did not consider

spectral HB. These issues have been addressed in the follow up theoretical work by using time domain (TD) simulations which have confirmed that strong FM is indeed the regime most favorable for laser operation (i.e., the regime with the lowest threshold and hence maximum emission efficiency [12]). A rationale for pseudo-random modulation was also obtained, although the advantage of randomization in terms of minimizing threshold was rather small, hence it was still not obvious if the laser would settle into this operational mode and not in some other local minimum of threshold power.

More recently, the first measurements of QCL combs using shifted wave interference Fourier transform spectroscopy (SWIFTs) were performed [13], in which the temporal profiles obtained [14], [15] were different from those predicted by the models. This method has been thoroughly studied and utilized by a number of groups [13], [14], [16]–[18]. While the strong FM and lack of pulses agrees with our models [11], [19], there is also a clear rapid AM of the intensity profile, which is something not predicted. Additionally, instead of rapid oscillations the instant frequency is linearly chirped with a period equal to the cavity roundtrip time. In [14] the linearity of the chirp was explicated as favoring residual dispersion compensation and a variational approach to the model presented in [11] shows a local minimum in the rate of change of the mode amplitudes. The fact that the linear chirp is indeed the preferred operational regime was explained on the basis of it reducing the energy dissipation due to in-plane current caused by population beating. However it does not explain the presence of AM. It is important in our view to provide additional rationale for the existence of the linearly chirped and pseudo-randomly amplitude modulated (AM) FC regime in QCLs.

There have been various published articles reporting similarly continuous-wave (CW), mode-locked, inter-band (quantum well, dot, dash) lasers exhibiting FM [20]–[24]. It is shown that a linear chirp FM is present, much like that seen in [14], [15], the major difference being the presence of strong AM in conjunction with FM for QCL FCs. However, in inter-band lasers the self-locked FM regime is less prevalent than in QCLs. It can be explained by the fact that while fast population beating is possible due to intra-band relaxation processes, the population dynamics are largely determined by the slower (nanosecond) inter-band recombination which dampens the population oscillations. Furthermore, the spatial HB is also dampened in inter-band quantum well lasers by diffusion, as the period of photo-induced depopulation grating is commensurate with the short wavelength in the material. Not surprisingly, the FC in these lasers, when they exist, are narrower than in QCLs. In quantum dot lasers, on the other hand, the diffusion is less of an issue, hence population oscillation is more robust and as a result, there is a somewhat stronger chance to obtain self-FM [25]. Another glaring difference between inter-band lasers and QCLs is of course that dispersion in the near IR, mid IR, and THz is vastly different.

In this work, after briefly reviewing the physics behind the FD and TD models developed previously (mostly included in the supplementary) we perform theoretical analysis and numerical calculations which explore how the experimentally observed,

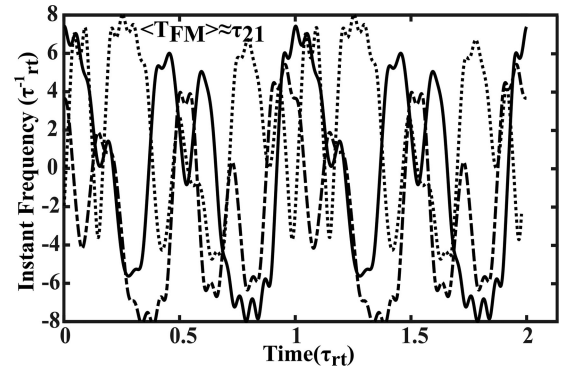


Fig. 1. Three results of independent runs of the FD model illustrating the pseudo-random instantaneous frequency modulation.

linearly chirped, and intensity modulated FC signals can be generated by the QCL. We achieve this through three methods, two of which involve modifications of our previous models to show stability of the linear chirp regime; with results outlined in Section III. The third method uses simple analytical calculations that illustrate the instability of pulse trains and the favorability of a linear chirp with residual AM and is outlined in Section IV. We find that spatial HB gets significantly mitigated in the linearly chirped oscillating regime, and, that fast and moderate AM also has potential for reducing HB. We hope that this work helps to educate the QCL FC community on the importance of spatial HB and serves as a first step towards engineering the QCL FC output to exert some control over its performance characteristics.

## II. FREQUENCY AND TIME DOMAIN MODELS

The phenomenological explanation of the QCLs having a natural state of FM operation that produces phase stable FCs was first confirmed via a theoretical model [11] developed in the frequency domain using a set of perturbative solutions to the Maxwell Bloch equations. Here we briefly review this model and its main results. The amplitude of the  $n$ -th mode is described by a set of equations for the amplitude of the modes,  $A_n$

$$\frac{dA_n}{dt} = (G_n - 1)A_n - G_n \sum A_m A_k A_l^* B_{kl} C_{kl} \kappa_{klmn} \quad (1)$$

The reader can refer to Section I of the supplementary file for a basic explanation of the equation (1) or reference [11] for a more detailed explanation. It is important to highlight the key difference between QCLs and other lasers, namely that for a QCLs,  $\tau_{21}/\tau_{rt} \ll 1$  as opposed to  $\tau_{21}/\tau_{rt} \gg 1$ , which is the case for semiconductor diode or solid state lasers. Therefore significant four-wave mixing (FWM) occurs, however, unlike the diode or solid state lasers, conventional mode-locking is still extremely difficult as mentioned previously. Despite this, the QCL still manages to lock a phase relation between the individual lines in the FC.

For a typical free running QCL, the FD model produces a nearly time independent intensity as well as a pseudo-random FM emission. Pseudo in that the FM is periodic with the round trip time, yet strongly irregular on shorter time scales, see Fig. 1. Successive results of the FD model first appear uncorrelated,

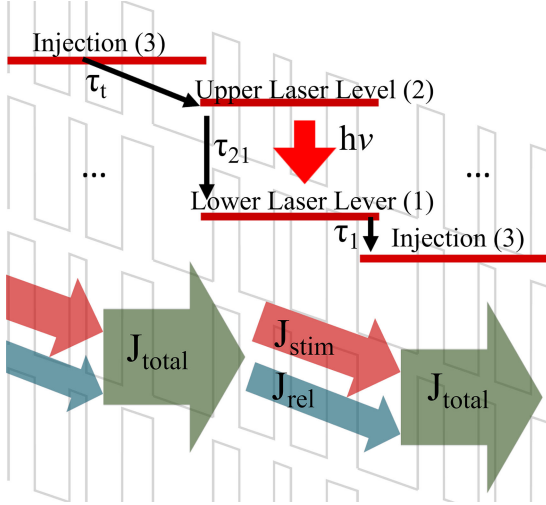


Fig. 2. Drawing of levels in one period of QCL with all the relevant times, and dissection of current, recycled through the periodic structure.

but each possess a central oscillation period,  $T_{fm}$ , commensurate with the gain recovery lifetime,  $\tau_{21}$ , and an amplitude commensurate with the gain bandwidth. At the time of writing [11], the explanation of pseudo-randomness was not given, but one can argue that the random nature of the FM is indeed a preferred operating regime of a free running QCL with a well-compensated dispersion. What is meant as the preferred operating regime is the regime which has the lowest threshold, or that in which the photons, on average, experience the highest net gain as they pass through the active region. This concept of maximum emission is not a new approach and is described thoroughly in [12]. This lowest threshold operation is achieved when spectral HB is mitigated by sweeping the gain and thus saturating the gain evenly. Spatial HB is mitigated via frequency mismatch of the counter-propagating waves that are present in a Fabry-Pérot cavity. We show later that the introduction of AM also potentially reduces spatial HB. The actual shape of the time domain profile will be determined by the level of influence of spectral and spatial HB, and which mechanism dominates. Due to the presence of a slow modulating linear ramp we suggest in this paper that spatial HB plays a more significant role.

To further understand the dynamics of the FC producing QCL we developed a rigorous TD model [19] where we describe the effects of FM by approximating the gain dynamics with the optical Bloch equations for an inhomogeneously broadened system. We describe the system using three levels as shown in Fig. 2: the injection level (level 3), upper laser level 2 (ULL), lower laser level 1 (LLL), then followed by the injection level again in the next period. The lifetimes of the ULL, LLL, and injection into ULL from level 3 are  $\tau_{21}^{-1}$ ,  $\tau_1^{-1}$ , and  $\tau_t^{-1}$  respectively. After showing that for a modulation that is slower than the coherence time, the Bloch equations can be simplified into the rate equations [26], we are essentially left with a set of  $N$  equations that take into account the effects of time dependent detuning  $\Delta\omega^{(n)}(t) = \omega_{fm}(t) - \omega_0^{(n)}$ . Here,  $n$ , indicates the  $n$ -th group of intersubband transitions centered at the resonant frequency

$\omega^{(n)}$ , thus taking into account inhomogeneous broadening,

$$\frac{d}{dt}N_{21}^{(n)}(z, t) = \frac{2N_o}{\tau_{21}} - \frac{2N_{21}^{(n)}(z, t)}{\tau_{21}} \left[ 1 + I(z, t)/I_{sat}^{(n)}(t) \right] \quad (2)$$

where  $I(z, t)$  is the intensity,  $N_{21}$  is the population inversion, and  $I_{sat}(z, t)$  is the saturation intensity. In order to take into account spatial HB, the inter-cavity radiation is placed in a Fabry-Pérot cavity and the counter propagating waves are realized via a spatial and temporal dependence of the intensity. The laser gain coefficient is then expressed as,  $\gamma(z, t) = \sum_{n=1}^{N_m} \sigma_{21}^{(n)}(\omega)N_{21}^{(n)}$ ,

where  $\sigma_{21}^{(n)}(\omega)$  is the effective emission cross-section (that includes the waveguide confinement factor) of the  $n$ -th group of transitions. In each period of the QCL the current density injected into the ULL then splits into two current densities – one  $J_{stim} \sim \gamma(z, t)I(z, t)$  is the current associated with the stimulated emission and the other current density,  $J_{rel}$ , is associated with mostly nonradiative relaxation of the ULL, see Fig. 2. Therefore, the maximum emission regime with the lowest threshold occurs when the stimulated current flowing through the entire laser structure is maximized, i.e., when the spatial and temporal average of the gain experienced by the photons,

$$\bar{\gamma} = \frac{\langle I(z, t)\gamma(z, t) \rangle_{z, \tau}}{\langle I(z, t) \rangle_{z, \tau}} \quad (3)$$

reaches a maximum. Refer to [19] for a more detailed description of the time-domain model and its results for both THz and long wave IR QCLs.

We now have the tools to present various operation scenarios to the time-domain model, which has been built to resemble the properties of a real world QCL by inhomogeneously broadening the gain bandwidth and introducing generally accepted specifications given in [19].

### III. LINEAR CHIRP IN FD AND TD MODELS

As the QCL FC output lacks pronounced pulses, traditional methods used to measure the time dependent emission are hard to employ as they rely on non-linear measurements which require high-intensity. However, development of SWIFTS [13] has given access to the phase separation of the FCs without employing optical nonlinearity. (Of course, square law detection in SWIFTS is by itself a nonlinear process which gives us possibility to obtain temporal shapes.) Results from this technique give time-dependent wave forms that were somewhat unexpected [14], [15]. Contrary to dynamics predicted by the time and frequency domain models, they incorporated a modulated intensity and a ramp-like FM, as shown in Figs. 3(c) and (d). These results seem to contradict those produced by the FD model. However, it should be noted that results from [11] were produced from low amplitude modes with randomized phases and neither spectral HB nor dispersion were incorporated.

Now we attempt to explain the disparity between our models and real world experiments, which will amount to weighting the influence of spectral HB. First we characterize the efficiency of a spectrally broadened QCL, via our TD model utilizing time



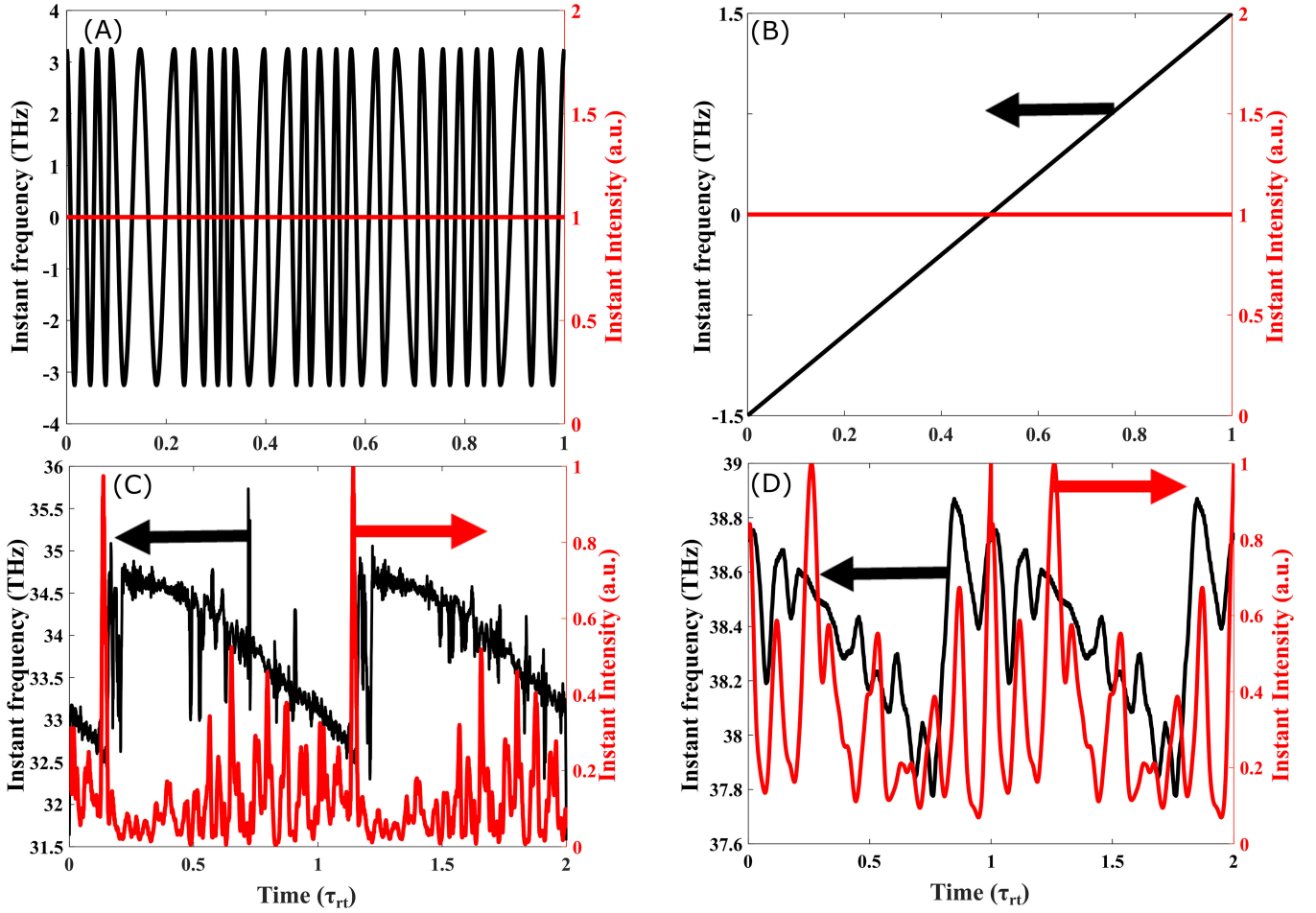


Fig. 3. An example of (A) a pseudo-random instantaneous frequency and (B) a frequency chirp produced for the TD model. (C) Time profile measurements of a FC QCL from [14]. (D) Time domain measurements of a FC QCL from [15].

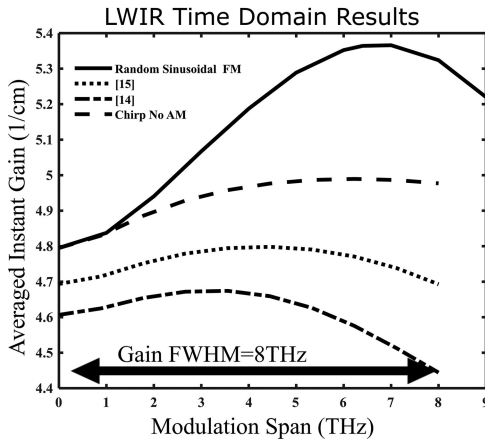


Fig. 4. The effective gain  $\bar{\gamma}$  vs modulation span results from the TD model for sinusoidal FM, experimental FM, and a frequency chirp.

profiles obtained from SWIFTS measurements [15] and [14], see Fig. 4. The data labeled in Fig. 4 as [15] and [14] were obtained by simply inputting the time domain signal from experiment into our model, incorporating strong inhomogeneous broadening,

and increasing the span at which the frequency reaches. Due to the AM present in experimental signals, both [15] and [14] produce gain values significantly lower than those present with pseudo-random sinusoidal FM signals. This is shown by the data labeled “Chirp No AM”, which from a lack of AM, shows that a frequency chirp is generally comparable to pseudo-random operation regime. Therefore, AM in this scenario results in a decreased gain, which may be contrary to reality. When comparing the linear frequency chirp to the pseudo random FM we see that because the period of the chirp is slow (the cavity roundtrip time) the gain is very low due to significant presence of spectral HB.

Hence it is reasonable to conclude that the spectral HB does not play a significant role in the experimentally tested QCLs. This appears a bit counterintuitive, especially for lasers with two different active periods, and requires extremely short intra-subband scattering times on the scale of 100 fs or even less for broad band lasers, but the presence of spectral HB was never confirmed by literature. Therefore, we have studied the influence of inhomogeneous broadening on the preferred operating regime. As shown in Fig. 5, a chirped FM regime is superior to the pseudo-random regime when the total bandwidth  $\Delta B_{TOT}$  is close to the homogeneous bandwidth  $\Delta B_H = 1/2\pi\tau_{coh}$ . We evaluate the

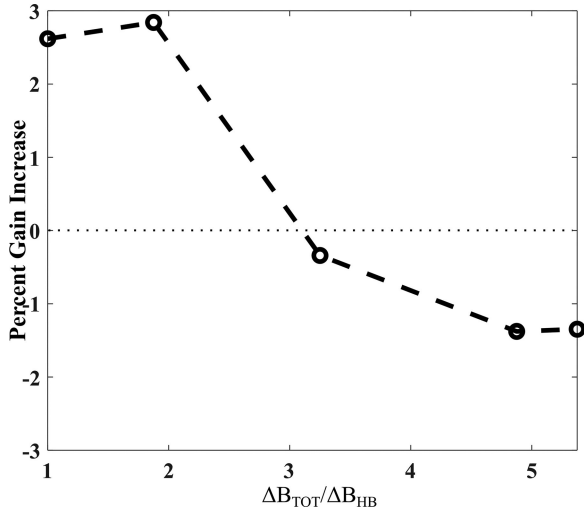


Fig. 5. Percent increase of the gain vs inhomogeneous broadening using a chirped FM as compared to a pseudorandom, faster FM.

values of the averaged gain experienced by photons (3) for the chirped  $\bar{\gamma}_{ch}$  and pseudo-random FM  $\bar{\gamma}_{pr}$  cases (for the same average laser power) and then plot the relative difference between them in percentage points  $\Delta\bar{\gamma} = (\bar{\gamma}_{ch} - \bar{\gamma}_{pr})/\bar{\gamma}_{pr} \times 100\%$ , the y-axis of Fig. 5. It can be seen that as long as the amount of inhomogeneous broadening is insignificant, the chirped FM appears to be the most favorable regime of QCL operation, but once inhomogeneous broadening increases the spectral hole burning reduces the gain for the chirped regime and the pseudo-random FM becomes preferred. While this difference is only a few percent, this small difference in efficiency is sufficient to make the linear chirp a preferred operating regime. This leads us to conclude that if the QCL does not suffer significantly from spectral HB, the frequency chirp may lead to a lower level of spatial HB and be dominant.

As mentioned above, absence of spectral HB in a broad gain QCL has not been fully explained yet. One can argue that if the inhomogeneous broadening is caused by variation of the active region thicknesses (whether intentional, as in a two-active region QCLs, or not) the fact that the same current flows through the different active regions prevents spectral hole formation. Whether the current is continuous on sub-picosecond scale (i.e., there is no fluctuating charge build-up in the injector) needs to be studied. It is more difficult to explain what prevents spectral hole formation if the active regions are non-uniform in the plane of growth, and the only reasonable assumption is then that when the growth is of sufficiently high quality that this non-uniformity is avoided. However, the experimental data supported now by our TD model strongly indicates that spectral HB appears not to be a defining factor and it is precisely this fact that makes a chirped FM the lowest threshold operating regime for a free running QCL.

The above TD results indicate that linear chirp is indeed a viable operating mode but it is not clear how stable it is. To study this we go back to the FD model and introduce initial conditions where the amplitudes and phases are similar to [14],

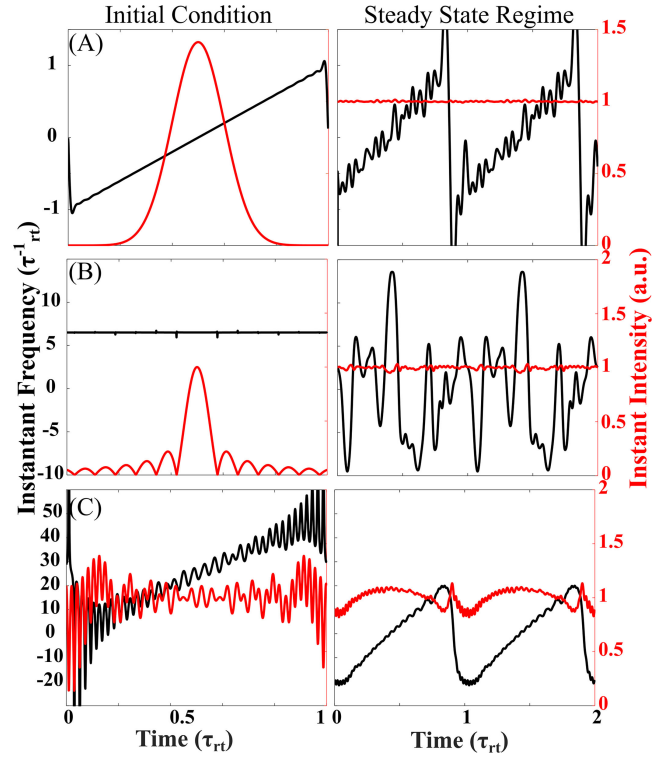


Fig. 6. Initial conditions and FD model results of three scenarios. (A) Pulse waveform with equal phases. (B) A broadband chirped FM waveform with quadratic phase relation. (C) A Chirped pulse that is narrowband.

[15], i.e., quadratic in time and broadband modes. We then run the model with chirped initial conditions under the presence of noise and see that indeed this mode of operation is stable. This stability is manifested by the FD model maintaining ramp-like instantaneous frequency after many iterations and further strengthened by the instability of a pulsed initial condition.

Three scenarios, shown in Fig. 6, have been tested for stability in a fast saturable gain. The first being a pulse with frequency chirp, the second equally phased modes (i.e., short pulse), and the third a broadband frequency chirp. As can be seen by comparing the first column (initial conditions) to the second (steady state regime), the FD model favors smooth CW radiation, regardless of the initial condition. In the first row, a chirped pulse was given to the FD model which retains its frequency chirp, although with a very narrow band, and smooths the pulse amplitude to be CW. In the second row a pulse is rapidly smoothed into CW radiation as predicted by [11]. However, introduction of a wideband, frequency chirped signal obviously shows stability in the phase relations between the modes, as shown in row 3. Interestingly, the data produced from the FD for a frequency chirp introduces residual AM that is correlated with the instantaneous frequency, much like what is seen in experiment (Fig. 3(c)), namely a spike in the intensity as the frequency undergoes a rapid negative slope. Thus, according to the FD model, while a short pulse (strong AM) is not stable and will always be smoothed, a long pulse or weak AM and a linear frequency chirp is. In the presence of some external influence forcing the initial phase relation between modes to be quadratic

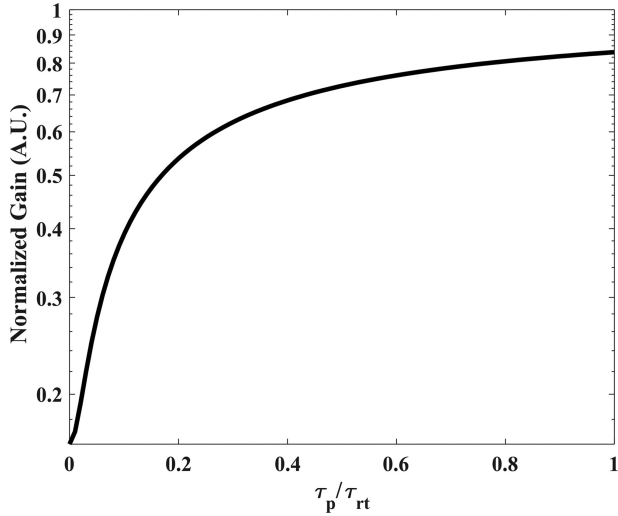


Fig. 7. Normalized averaged gain experience by a pulse versus the pulse length normalized to the cavity roundtrip time.

in addition to very little spectral HB, a stable, linear frequency chirp emerges as a stable regime. It should be noted that while the FC is by no means perfectly periodic, the periodicity is good enough for spectroscopy. For more discussion on the noise involved in QCL FC refer to [27].

#### IV. ANALYTICAL STUDY IN TIME DOMAIN SPATIAL HOLE BURNING AND INSTANT GAIN

In order to further investigate the possibly infinite number of operation scenarios of the laser, considering both amplitude and frequency modulation, we provide analytical derivations of the effect of spatial HB and gain saturation. We use these to understand which operation regimes of the laser are favorable. Thus we must devise a proper figure of merit to compare these operation regimes, we calculate the gain experienced by the photon,  $\bar{\gamma} = \langle \gamma(z, t) p'(z, t) \rangle_{z, t} / \bar{p}$ , where  $p'(z, t) = \langle p(z, t) \rangle_{\tau_{21}} = \frac{1}{\tau_{21}} \int_{-\infty}^t p(z, \tau) e^{\frac{\tau-t}{\tau_{21}}} d\tau$  is the intracavity intensity averaged by the upperstate lifetime and normalized to the saturation power density. The gain medium acts as an “integrator” with the characteristic time equal to the gain recovery time, i.e., it responds to the averaged power as  $\gamma(z, t) = \gamma_0 / (1 + p'(z, t))$ . Additionally, we will introduce the averaged spatial variance of the power,  $\sigma_{av}^2 = \langle (p(z, t)' - \bar{p})^2 \rangle_{z, \tau}$ , as a measurement of spatial HB.

First let us consider how the mode-locked pulse is not favored in the presence of a fast saturable gain. Let us now assume that a short pulse of duration  $\tau_p$  propagates inside the cavity. We see that when we plot the gain versus pulse length for a normalized average power with realistic ratio of  $\Gamma = \tau_{21} / \tau_{rt} = 1/40$ , the longer the pulse, the higher the gain. Obviously, for a fast saturable gain ( $\Gamma \ll 1$ ), the longer the pulse the more efficient the laser. Refer to the supplementary Section II for a detailed derivation of Fig. 7.

Now we turn to analyze spatial HB in the cavity under various operational scenarios while including both amplitude

and frequency modulation. First we show that spatial HB in fact reduces laser efficiency as holes in the gain cause excess non-radiative decay, and thus will not emerge as the dominant operation regime. If the uniform unsaturated gain in the medium is  $\gamma_0$ , it saturates as  $\gamma(z, t) = \gamma_0 / (1 + p(z, t))$ . The average gain experienced by the photon is then

$$\begin{aligned} \bar{\gamma} &= \frac{\langle \gamma(z, t) p(z, t) \rangle_{z, t}}{\bar{p}} = \frac{\gamma_0}{\bar{p}} \left\langle \frac{\bar{p} + \delta p(z, t)}{1 + \bar{p} + \delta p(z, t)} \right\rangle_{z, t} \\ &\approx \frac{\gamma_0}{1 + \bar{p}} \left[ 1 - \frac{\langle \delta p^2 \rangle_{z, t}}{\bar{p}(1 + \bar{p})^2} \right] \approx \frac{\gamma_0}{1 + \bar{p}} [1 - \bar{p}\sigma^2] \end{aligned}$$

where the variance is defined as  $\sigma^2 = \langle \delta p^2(x, t) \rangle_{t, z} / \bar{p}^2$ . Obviously as the power variance, our figure of merit, is increased the averaged gain seen by the photon decreases. For the single standing wave mode one can calculate  $\sigma^2 = \langle (X - \mu)^2 \rangle = \frac{1}{2\pi} \int_0^{2\pi} (\sin^2(x) - 1/2)^2 dx = \frac{1}{8}$ .

This is a worst-case scenario and thus we look for a variance smaller than this value to show a marked mitigation of spatial HB and thus an increase in the laser efficiency and a more probable operation mode.

To get an idea of the significant factors controlling the power variance of the intracavity spatial intensity distribution we turn to analytical calculations of the FM signals interfering in a Fabry-Pérot cavity. For the following calculations we consider only an FM signal where the frequency modulation is a deterministic cosine with modulation index  $\beta = \Delta\omega / \omega_{fm}$ , where  $\Delta\omega$  is the bandwidth of the gain/or frequency deviation of the FM signal, and  $\omega_{fm}$  is the angular frequency of the FM signal. We begin with two counter propagating waves

$$\begin{aligned} E(z) &= \frac{E_0}{2} \exp \left\{ \begin{array}{l} -j\omega_0(t + \Delta t/2) \\ -j\beta \cos[\omega_{fm}(t + \Delta t/2)] \end{array} \right\} \\ &+ \frac{E_0}{2} \exp \left\{ \begin{array}{l} -j\omega_0(t - \Delta t/2) \\ -j\beta \cos[\omega_{fm}(t - \Delta t/2)] \end{array} \right\} \end{aligned} \quad (4)$$

and are able to calculate the power variance as  $\sigma^2 = \langle (\frac{1}{2} \cos(\omega_0 \Delta t + \beta \sin \omega_{fm} t \sin \omega_{fm} \Delta t/2))^2 \rangle = \frac{1}{8}$ , i.e., the same as no modulation. However, when averaging over the period of modulation and assuming that the period of modulation is commensurate with the upperstate lifetime, we see that the power variance decreases significantly with the modulation index, see Fig. 8. Calculating the averaged variance can be approximated with an infinite sum

$$\begin{aligned} \sigma_{av}^2 &= \frac{1}{T} \int_0^T \left[ \frac{1}{2} J_0(\beta \sin \omega_{fm} \Delta t/2) \cos(\omega_0 \Delta t) \right]^2 d\Delta t \\ &\approx \frac{1}{T} \int_0^T \frac{1}{8} \left[ \sum_{k=0}^{\infty} (-1)^k \frac{[(\beta \sin \omega_{fm} \Delta t/2)^2 / 4]^k}{(k!)^2} \right]^2 d\Delta t \end{aligned} \quad (5)$$

This shows the power of the modulation index, and offers the conclusion that a large frequency deviation gives a small intracavity power variance. As we have seen a linear frequency chirp in experiment, it is also useful to calculate the variance

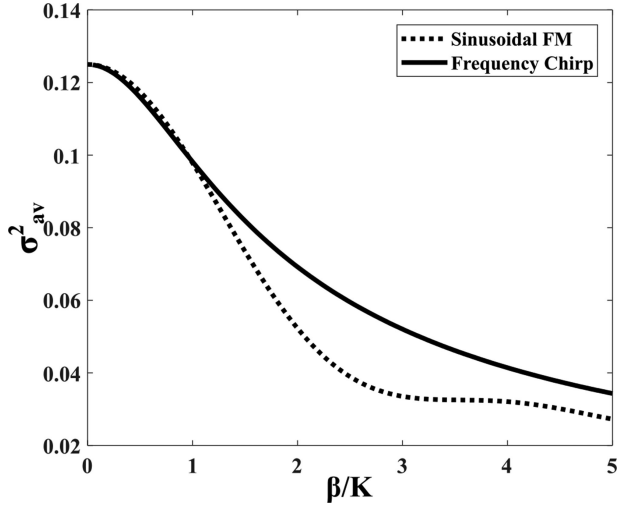


Fig. 8. Averaged power variance versus modulation index or  $K$  for a deterministic, sinusoidal FM signal and a frequency chirp with a period equal to the cavity time.

of this chirp versus the span of frequency. Starting off with an equation similar to (4) including a linear term rather than a cosine in the phase we obtain for the power variance

$$\sigma^2 = \langle \delta \bar{S}^2 \rangle_{z,\tau} = \frac{1}{8} \left\langle \frac{1}{(Kz)^2 + 1} \right\rangle_{z=0..1} = \frac{1}{8} \frac{\arctan(K)}{K} \quad (6)$$

where  $K$  is the FM strength similar to the modulation index,  $K = \Delta\omega\tau_{21}$ . Please refer to the supplementary file for a complete derivation of Equation (6), we include the results from (5) and (6) on Fig. 8.

There is a subtle difference between the two scenarios (sinusoidal FM and frequency chirp), namely that, regarding the sinusoidal FM, the oscillation must be comparable to the upper level lifetime as the averaging is implicitly over the period of frequency modulation. Additionally, FM oscillations with a frequency faster than the averaging time ( $\tau_{21}$ ) will not help to improve the power variance, and slower oscillations may degrade performance. With a linear frequency chirp scenario, the longer the upper state lifetime, the better the performance, regardless of the implicit period of the waveform. Additionally, the longer the span of the FM, the better the performance. Thus, while the frequency chirp looks to be worse than the sinusoidal FM in Fig. 8, with the right specifications a frequency chirp could be the best performer.

Now, as mentioned previously, there have been FC generating QCLs reported that have shown moderate AM in addition to FM. In an attempt to explain this, we calculate the power variance of a signal with deterministic, sinusoidal AM

$$E(z, t) = \frac{E_0}{2} \exp(-j\omega_0 t) \times \left\{ \begin{array}{l} \cos[\omega_m(t + \Delta t/2)] \exp[-j\omega_0 \Delta t/2] \\ + \cos[\omega_m(t - \Delta t/2)] \exp[+j\omega_0 \Delta t/2] \end{array} \right\} + c.c.$$

Squaring the electric field and taking the variance we see that  $\sigma^2 = \frac{1}{T_m} \int \sigma^2(\Delta t) d\Delta t = \frac{3}{16}$ . The unaveraged power variance in fact increases, effectively making spatial HB worse. However, we can see that if averaged by the oscillation period, or under the condition that the oscillation frequency is commensurate with the gain recovery time, the averaged power variance is halved which surprisingly leads to a variance lower than that of pure FM (for low modulation index).

$$\sigma^2 = \left\langle \frac{1}{4} \cos^2(\omega_m \Delta t) \cos^2(\omega_0 \Delta t) \right\rangle_{\Delta t} = \frac{1}{16}$$

Thus, in some cases, AM can help to improve spatial HB as long as the oscillations are rapid enough to be averaged by the active medium. AM can be especially helpful when the FM undergone by the QCL is effectively at a low modulation index ( $\beta$ ), as FM alone can beat out AM at a higher modulation index. It is apparent that the functions controlling the standard deviation are multiplicative and thus mitigation of spatial HB from AM and FM will act as such. It is now useful to add randomization to our sinusoidal AM signals calculations, in an attempt to further lower the variance. Fig. 9 below presents the variance for different combinations of deterministic and random sinusoidal modulation. Additionally, variance measurements were performed on data presented in [14] and [15], showing that the spatial HB is in fact mitigated in both, with [14] being slightly better, possibly from the faster AM.

So, what is the reason behind the persistent amplitude modulation that is always observed? To answer this question one should realize that the phase locking is achieved via population beating in the cavity and if the amplitude of the signal is constant the phase locking cannot be robust. Thus at least residual AM is necessary to maintain FC against deleterious effects of dispersion as well as all kinds of noise.

When considering the frequency modulation index of both [14] and [15] we see that they span a peak frequency deviation of  $\beta = A_m/f_{FM} \approx 2 \text{ THz}/10 \text{ GHz} = 200$ , with this high of a modulation index it is easy to see how spatial HB is mitigated. However, this calculation of modulation index is under the assumption that the fastest frequency in the FM signal is  $1/\tau_{rt}$  which is most likely not accurate, thus modulation index is most likely lower than 200 necessitating some introduction of AM. Considering the randomized AM and FM data, we must note that, unlike the derivation described earlier, the AM is a sinusoid added to a CW wave, so that the average of the electric field is  $1/\sqrt{(2)}$  rather than zero and the modulation span  $A_{AM} = 0.75$ . As these are randomized we can no longer calculate the variance analytically, however we are able to show that further randomization of the frequency modulation signal lowers spatial HB, explaining the apparent noise in the FM signals of [14], [15]. We also show, in Fig. 9(b), the variance measurements for a simulated frequency chirp, both with and without a pulse, as well as experimental data. It is reassuring to note that the data presented here greatly resembles the analytical solution presented in Fig. 8. As can be seen in Fig. 9(b) the experimental data from [14], [15] lies between a chirped pulse and a chirped frequency without a pulse.



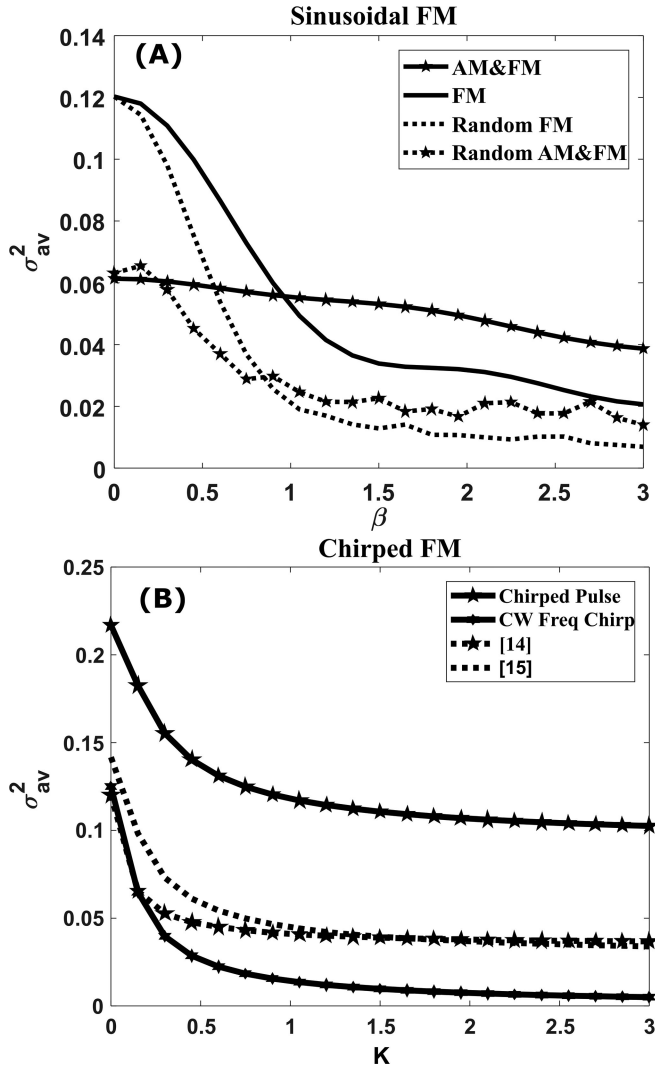


Fig. 9. (A) Averaged variance measurements of various sinusoidal FM signals. (B) Averaged variance measurements of various linearly chirped FM signals.

Therefore, a high frequency modulation index is critical to lowering variance with FM in the case of sinusoidal modulation and a high upper state lifetime and wide bandwidth are critical to lowering variance with a chirped frequency modulation. Fast AM does indeed decrease the average variance as long as it is faster than the gain recovery time. When both AM and FM are present the derivation shows to be multiplicative, thus the dominate effects depend on the modulation index and it is possible for the AM to compensate for peaks due to instant frequency matching in the cavity.

## V. CONCLUSION

In this work we have used two different models of QCL operation, one in the FD and one in the TD with the goal of explaining the experimentally observed characteristics of the free running QCL operating in the FC regime. Using the TD model, both analytically and numerically, we have shown that experimentally observed, chirped emission with partial AM does

reduce the laser threshold by mitigating spatial HB. Furthermore as long as spectral HB does not take place, the linear chirp shows a threshold that is lower than any other FM regime.

Using a self-consistent FD model, we have shown that an experimentally observed, linearly chirped signal is stable, i.e., once this regime is achieved it remains robust, unlike other regimes tested by us. What still remains unresolved is exactly how this linearly chirped regime develops from the noise when the QCL turns on, although presence of residual group delay dispersion seems to be a logical culprit. Hopefully our continuing work will eventually lead us to a full understanding of QCL FCs and deliver a powerful set of tools for the real world engineering of mid-IR and THz FCs with predictable characteristics.

## ACKNOWLEDGMENT

The authors would like to thank M. Singleton and J. Faist of ETH for the data provided and numerous discussions.

## REFERENCES

- [1] T. Udem, R. Holzwarth, and T. W. Hänsch, "Optical frequency metrology," *Nature*, vol. 416, no. 6877, pp. 233–237, 2002.
- [2] A. Schliesser, N. Picqué, and T. W. Hänsch, "Mid-infrared frequency combs," *Nat. Photon.*, vol. 6, no. 7, pp. 440–449, 2012.
- [3] R. Fork, B. Greene, and C. V. Shank, "Generation of optical pulses shorter than 0.1 psec by colliding pulse mode locking," *Appl. Phys. Lett.*, vol. 38, no. 9, pp. 671–672, 1981.
- [4] T. M. Fortier, A. Bartels, and S. A. Diddams, "Octave-spanning Ti: Sapphire laser with a repetition rate >1 GHz for optical frequency measurements and comparisons," *Opt. Lett.*, vol. 31, no. 7, pp. 1011–1013, 2006.
- [5] I. Galli *et al.*, "Absolute frequency measurements of CO<sub>2</sub> transitions at 4.3  $\mu\text{m}$  with a comb-referenced quantum cascade laser," *Mol. Phys.*, vol. 111, no. 14/15, pp. 2041–2045, 2013.
- [6] T. J. Kippenberg, R. Holzwarth, and S. Diddams, "Microresonator-based optical frequency combs," *Science*, vol. 332, no. 6029, pp. 555–559, 2011.
- [7] N. Leindecker, A. Marandi, R. L. Byer, and K. L. Vodopyanov, "Broadband degenerate OPO for mid-infrared frequency comb generation," *Opt. Express*, vol. 19, no. 7, pp. 6296–6302, 2011.
- [8] J. Faist, F. Capasso, D. L. Sivco, C. Sirtori, A. L. Hutchinson, and A. Y. Cho, "Quantum cascade laser," *Science*, vol. 264, no. 5158, pp. 553–556, 1994.
- [9] A. Hugi, G. Villares, S. Blaser, H. Liu, and J. Faist, "Mid-infrared frequency comb based on a quantum cascade laser," *Nature*, vol. 492, no. 7428, pp. 229–233, 2012.
- [10] D. Burghoff *et al.*, "Terahertz laser frequency combs," *Nat. Photon.*, vol. 8, no. 6, pp. 462–467, 2014.
- [11] J. Khurgin, Y. Dikmelik, A. Hugi, and J. Faist, "Coherent frequency combs produced by self frequency modulation in quantum cascade lasers," *Appl. Phys. Lett.*, vol. 104, no. 8, 2014, Art. no. 081118.
- [12] C. Tang and H. Statz, "Maximum-emission principle and phase locking in multimode lasers," *J. Appl. Phys.*, vol. 38, no. 7, pp. 2963–2968, 1967.
- [13] D. Burghoff *et al.*, "Evaluating the coherence and time-domain profile of quantum cascade laser frequency combs," *Opt. Express*, vol. 23, no. 2, pp. 1190–1202, 2015.
- [14] M. Singleton, P. Jouy, M. Beck, and J. Faist, "Evidence of linear chirp in mid-infrared quantum cascade lasers," *Optica*, vol. 5, no. 8, pp. 948–953, 2018.
- [15] D. Burghoff, unpublished.
- [16] J. Hillbrand, A. M. Andrews, H. Detz, G. Strasser, and B. Schwarz, "Coherent injection locking of quantum cascade laser frequency combs," *Nature Photon.*, vol. 13, no. 2, pp. 101–104, 2019.
- [17] J. Mandon, G. Guelachvili, and N. Picqué, "Fourier transform spectroscopy with a laser frequency comb," *Nature Photon.*, vol. 3, no. 2, pp. 99–102, 2009.



- [18] F. Cappelli *et al.*, "Retrieval of phase relation and emission profile of quantum cascade laser frequency combs," *Nat. Photon.*, vol. 13, pp. 562–568, 2019.
- [19] N. Henry, D. Burghoff, Q. Hu, and J. B. Khurgin, "Temporal characteristics of quantum cascade laser frequency modulated combs in long wave infrared and THz regions," *Opt. Express*, vol. 26, no. 11, pp. 14201–14212, 2018.
- [20] R. Rosales *et al.*, "High performance mode locking characteristics of single section quantum dash lasers," *Opt. Express*, vol. 20, no. 8, pp. 8649–8657, 2012.
- [21] M. Gioannini, P. Bardella, and I. Montrosset, "Time-domain traveling-wave analysis of the multimode dynamics of quantum dot Fabry–Perot lasers," *IEEE J. Sel. Topics Quantum Electron.*, vol. 21, no. 6, 2015, Art. no. 1900811.
- [22] K. Sato, "Optical pulse generation using fabry-Pe/spl acute/rot lasers under continuous-wave operation," *IEEE J. Sel. Topics Quantum Electron.*, vol. 9, no. 5, pp. 1288–1293, Sep./Oct. 2003.
- [23] M. Dong, N. M. Mangan, J. N. Kutz, S. T. Cundiff, and H. G. Winful, "Traveling wave model for frequency comb generation in single-section quantum well diode lasers," *IEEE J. Quantum Electron.*, vol. 53, no. 6, Dec. 2017, Art. no. 2500311.
- [24] P. Bardella, L. L. Columbo, and M. Gioannini, "Self-generation of optical frequency comb in single section quantum dot Fabry-Perot lasers: A theoretical study," *Opt. Express*, vol. 25, no. 21, pp. 26234–26252, 2017.
- [25] A. Fiore *et al.*, "Carrier diffusion in low-dimensional semiconductors: A comparison of quantum wells, disordered quantum wells, and quantum dots," *Physical Rev. B*, vol. 70, no. 20, 2004, Art. no. 205311.
- [26] N. Henry, D. Burghoff, Y. Yang, Q. Hu, and J. B. Khurgin, "Pseudorandom dynamics of frequency combs in free-running quantum cascade lasers," *Opt. Eng.*, vol. 57, no. 1, 2017, Art. no. 011009.
- [27] J. B. Khurgin, N. Henry, D. Burghoff, and Q. Hu, "Linewidth of the laser optical frequency comb with arbitrary temporal profile," *Appl. Phys. Lett.*, vol. 113, no. 13, 2018, Art. no. 131104.

**Nathan Henry** graduated from the University of New Mexico in 2012. He received the Ph.D. degree in electrical engineering from Johns Hopkins University, Baltimore, MD, USA, in 2015, under the tutelage of Jacob B. Khurgin. He was with Night Vision and Electronic Sensors Directorate, where he was involved in fabrication techniques for strained-layer superlattice infrared detectors. His research interest includes quantum cascade lasers.

**David Burghoff** received the Ph.D. degree in electrical engineering from the Massachusetts Institute of Technology (MIT), Cambridge, MA, USA, in 2014, for which he was awarded the Jin-Au Kong Doctoral Thesis Award. Since 2015, he has been a Research Scientist with the Research Laboratory of Electronics at MIT. Since 2018, he has been a Professor with the University of Notre Dame, Notre Dame, Indiana. His research interests include intersection of quantum nanostructures, long-wavelength photonics, ultrafast optics, and computationally assisted spectroscopy.

**Qing Hu** received the Ph.D. degree in physics from Harvard University, Cambridge, MA, USA, in 1987. He joined the Massachusetts Institute of Technology in 1990, where he is a Distinguished Professor with the Electrical Engineering and Computer Science Department. He has made significant contributions to physics and device applications over a broad spectrum, from millimeter wave, terahertz (THz), to infrared frequencies. Among those contributions, the most distinctive is his development of high performance THz quantum cascade lasers.

**Jacob B. Khurgin** received the Ph.D. degree from the Polytechnic University of New York, New York City, New York, USA. He has been a Professor of Electrical and Computer Engineering, Johns Hopkins University (JHU), Baltimore, MD, USA, since 1988. Prior to that, he was a Senior Member of Research Staff with Philips NV where he developed various display components and systems including 3-D projection TV and visible lasers pumped by electron beam. In his 30 years with JHU, he had made important contributions in the fields of nonlinear optics, semiconductor optoelectronic devices, quantum-cascade lasers, optical communications, terahertz technology, slow light, plasmonics, opto-mechanics, and fundamental condensed matter physics. He had authored more than 300 technical papers, 500 conference presentations, five book chapters, and held 40 patents. His research interests include optical and electronic solid state devices. Prof. Khurgin is a Fellow of American Physical Society and Optical Society of America.